Bifurcation control of a seizing human cortex

Mark A. Kramer,[1] Beth A. Lopour,[2] Heidi E. Kirsch,[3] and Andrew J. Szeri[1,2,*]
[1]*Program in Applied Science and Technology, University of California, Berkeley, California 94720, USA*
[2]*Department of Mechanical Engineering, University of California, Berkeley, California 94720, USA*
[3]*Department of Neurology, University of California, San Francisco, California 94143, USA*
(Received 9 September 2005; revised manuscript received 19 December 2005; published 27 April 2006)

We consider as a mathematical model of human cortical electrical activity a system of fourteen ordinary differential equations. With appropriate parameters, the model produces activity characteristic of a seizure. To prevent such seizures, we incorporate feedback controllers into the model dynamics. We show that three controllers—a linear feedback controller, a differential controller, and a filter controller—can be used to eliminate seizing activity in the model system. We show how bifurcations induced by the linear controller alter those present in the original dynamics.

DOI: 10.1103/PhysRevE.73.041928 PACS number(s): 87.19.La, 05.10.−a, 07.05.Dz, 07.05.Tp

I. INTRODUCTION

Epilepsy—chronic unprovoked seizures—affects over 2.5 million people in the USA [1]. Unfortunately, an estimated 20% of people with epilepsy do not respond to medications prescribed to control seizures [1]. For these patients, treatment options are more invasive. Some patients may choose to undergo resective surgery, in which surgeons remove the brain region responsible for seizure genesis—the epileptogenic zone. When the epileptogenic zone includes eloquent cortex (e.g., motor or speech cortex) resective surgery may not be safe, and the patient must consider alternative treatments. Brain electrical stimulation (BES) represents an important new treatment for intractable epilepsy. The most common—and only U.S. Food and Drug Administration (FDA) approved—BES method is vagus nerve stimulation. In this method, electrodes (attached to a battery powered computer implanted subcutaneously on the patient's chest wall) periodically deliver electrical pulses to the vagus nerve. This chronic stimulation of the vagus nerve is thought to affect brain regions (e.g., the thalamus) that might, in theory, increase cortical inhibition and thereby lessen or modulate seizures. Other, as yet experimental, BES methods target brain regions such as the cerebellum, caudate nucleus, and thalamus [2]. The physiological mechanisms by which these BES methods prevent or reduce seizures are unknown.

Seizures may also be aborted by direct electrical stimulation of the cortex. For example, cortical afterdischarges (seizure-like activity elicited by direct cortical electrical stimulation, used for brain mapping) may be arrested by applying brief bursts (0.3–2.0 s) of pulse stimulation (0.3 ms duration biphasic pulses delivered 50 times per second at 1.0–15.0 mA) to the cortex [3,4]. Others have found that biphasic pulses delivered at high frequencies (e.g., 200 Hz in [5]), moderate frequencies (e.g., 50 Hz in [6]), and low frequencies (e.g., 0.9 Hz in [6]) can reduce seizure activity. However, not all stimulation frequencies are appropriate. Moderate frequency (5–20 Hz) stimulation delivered for 5–12 s may, in fact, increase baseline epileptiform activity [7].

For cortical BES, there may exist optimal stimulation sites, transducers, and parameters for terminating seizures. Of course, the most important consideration for physicians and researchers is patient safety. Animal models of epilepsy may allow researchers to explore different BES methods that may pose unacceptable risks to human subjects. In [8], the authors show that small, uniform electric fields—directed from the soma to the apical dendrites—transiently suppress epileptiform activity in rat hippocampal slices *in vitro*. An improvement to this method is reported in [9], where the authors apply time varying electric fields via a continuous, proportional feedback algorithm to rat hippocampal slices *in vitro*. They find that this feedback controller reduces seizure-like activity with more success than the uniform electric fields.

Mathematical models provide another means to safely explore the effects of new BES techniques. Detailed models exist that describe the behavior of individual neurons during seizure [10]. To compare these model results with experimental data, researchers record single neuron activity and local field potentials from, for example, CA1 of the rat *in vitro* [11]. In humans, we can take advantage of a common clinical scenario: the use of subdural electrodes to record brain wave activity, including seizures, in patients undergoing surgery for intractable epilepsy. We may then compare the results of mathematical models with this electrocorticogram (ECoG) data recorded from the seizing human cortex. The relationship between the single neuron models and the ECoG data—which records the summed activity from neuronal populations—is not obvious. To facilitate a comparison with the observed data we consider a mathematical model of the mesoscopic cortical electrical activity.

Our goal in this work is a theoretical exploration of new BES techniques. In what follows, we apply three feedback controllers—a proportional controller, differential controller, and filter controller—to a mathematical model of human cortical electrical activity. Others have employed mathematical systems to model the effects of BES [12,13]. In those works, the authors consider the activity of individual neurons and networks of neurons. Here we implement a model of mesos-

*Electronic address: aszeri@me.berkeley.edu

TABLE I. Dynamical variable definitions for the dimensionless ODEs neural macrocolumn model. The dimensionless variables (left column) are defined in terms of the dimensional symbols (middle column) found in Table 1 of [21]. The variables are described in the right column. Subscripts e and i refer to excitatory and inhibitory, respectively.

Symbol	Definition	Description
$\tilde{h}_{e,i}$	$h_{e,i}/h^{\mathrm{rest}}$	Population mean soma dimensionless electric potential
$\tilde{I}_{ee,ie}$	$I_{ee,ie}\gamma_e/(G_e \exp(1) S^{\max})$	Total $e\to e$, $i\to e$ input to excitatory synapses
$\tilde{J}_{ee,ie}$	$\tau \frac{dI_{ee,ie}}{dt}\gamma_e/(G_e \exp(1) S^{\max})$	Time derivative of the total $e\to e$, $i\to e$ input to excitatory synapses
$\tilde{I}_{ei,ii}$	$I_{ei,ii}\gamma_i/(G_i \exp(1) S^{\max})$	Total $e\to i$, $i\to i$ input to inhibitory synapses
$\tilde{J}_{ei,ii}$	$\tau \frac{dI_{ei,ii}}{dt}\gamma_i/(G_i \exp(1) S^{\max})$	Time derivative of the total $e\to i$, $i\to i$ input to inhibitory synapses
$\tilde{\phi}_{e,i}$	$\phi_{e,i}/S^{\max}$	Long range (corticocortical) input to e,i populations
$\tilde{\psi}_{e,i}$	$\tau \frac{d\phi_{e,i}}{dt}/S^{\max}$	Time derivative of long range (corticocortical) input to e,i populations
$\tilde{t}$	t/τ	Dimensionless time

cale cortical electrical activity (a system of fourteen ordinary differential equations) and show how to make the model "seize" in Sec. II. In Sec. III we apply the linear proportional feedback controller to one model variable ($\tilde{h}_e$—the spatially averaged soma membrane potential of excitatory cortical neurons). We show that, when the controller gain exceeds a threshold value, the controller suppresses seizure-like oscillations occurring in the dynamics. The controller works through control of bifurcations; to make the discussion precise we make use of the taxonomy introduced in [14]. We discuss the types of bifurcations that both produce (subHopf/fold cycle) and destroy the large amplitude, stable oscillations characteristic of a seizure. In Secs. IV and V we apply a differential controller and filter controller, respectively, to the dynamics. We show that both controllers suppress seizure-like oscillations—although bifurcation analysis is not as readily performed for these controllers. In Sec. VII we discuss the results and possible future applications.

II. MODEL

In this section, we define the equations, variables, and parameters we employ to model the seizing human cortex. Ideally, one would describe human cortical electrical activity in terms of individual neurons. For example, such a model may consist of an interconnected network of physiologically accurate cortical neurons. To implement this model one would have to (at least) define the characteristics of each neuron (e.g., pyramidal or stellate, extent of dendritic branching, location), the connections between neurons, and the connections from other brain regions. Unfortunately, a complete description of human cortical physiology does not exist. Even if we approximate this complicated physiology, computational limits still make detailed simulations infeasible (although see [15,16]).

To avoid these difficulties we employ a mesoscale model of human cortical electrical activity. Two of the earliest mesoscale models were developed by Wilson and Cowan [17] and Freeman [18]. Here we employ a recent formulation first proposed by Liley, Cadusch, and Wright (LCW) in [19], and later expanded by others in [20–22]. To create this model, LCW spatially averaged the microscopic properties of individual neurons over cortical columns [23]. A cortical column represents the approximate cortical volume synapsed by the branching dendrites of subcortical input; it extends across the five layers of cortex (approximately 3 mm in depth) and has

TABLE II. Parameter values for the dimensionless ODEs neural macrocolumn model. The dimensionless symbols (first column) are defined in terms of the dimensional variables (second column) found in Table I of [21]. The variables are described in the third column and typical values are shown in the fourth column.

Symbol	Definition	Description	Typical Value
e,i		(As subscript) excitatory, inhibitory cell populations	
$\Gamma_{e,i}$	$\frac{G_{e,i}\exp(1)S^{\max}}{\gamma_{e,i}\lvert h_{e,i}^{\mathrm{rev}}-h^{\mathrm{rest}}\rvert}$	Influence of input on the mean soma membrane values	1.42×10^{-3}, 0.0774
$h_{e,i}^{0}$	$h_{e,i}^{\mathrm{rev}}/h^{\mathrm{rest}}$	Dimensionless cell reversal potential	–0.643, 1.29
$T_{e,i}$	$\tau\gamma_{e,i}$	Dimensionless neurotransmitter rate constant	12.0, 2.6
$\lambda_{e,i}$	$\tau\tilde{v}\Lambda_{ee,ei}$	Dimensionless characteristic corticocortical inverse-length scale	11.2, 18.2
$P_{ee,ie}$	$p_{ee,ie}/S^{\max}$	Subcortical input to e population	11.0, 16.0
$P_{ei,ii}$	$p_{ei,ii}/S^{\max}$	Subcortical input to i population	16.0, 11.0
$N_{e,i}^{\alpha}$	—	Total number of synaptic connections from distant e populations	4000, 2000
$N_{e,i}^{\beta}$	—	Total number of local e and i synaptic connections	3034, 536
$\tilde{g}_{e,i}$	$g_{e,i}h^{\mathrm{rest}}$	Dimensionless sigmoid slope at inflection point	–19.6, –9.8
$\tilde{\theta}_{e,i}$	$\theta_{e,i}/h^{\mathrm{rest}}$	Dimensionless inflection-point for sigmoid function	0.857, 0.857

a cortical surface area of approximately 2 mm^2. The cortical column (and not the neuron) is the smallest unit of activity in the mesoscale model [24]. We can easily compare the results computed from such mesoscale models with ECoG data, which is thought to record the summed electrical activity of cortical columns.

Here we employ a formulation of this mesoscale model developed in [22]. The (nondimensionalized) system consists of 14 stochastic partial differential equations (SPDEs) first-order in time and second-order in space, and 20 parameters. We showed in [22] that the model can approximate the electrical activity recorded from the seizing human cortex at certain parameter values. Specifically, we adjusted two model parameters: P_{ee}—the excitatory subcortical input to excitatory cortical neurons, and Γ_e—the strength of excitatory synaptic input to both excitatory and inhibitory cortical neurons. We chose to adjust these two parameters because both affect the excitation of the model, and a state of cortical hyperexcitation is characteristic of some seizures [25]. In addition, we have found that increases in Γ_e or P_{ee} depolarize h_e—the (dimensional) spatially averaged soma membrane potential of the excitatory cells; we define the relationship between $\tilde{h}_e$ and h_e, and between the other dimensionless model variables and their dimensional counterparts in Table I. Such an increase in h_e is thought to be an important control factor in inducing seizures [26,27].

We showed in [22] that large increases (greater than 2200%) in P_{ee} and small decreases (as small as 12%) in Γ_e produced seizure-like activity in the (dimensionless) variable $\tilde{h}_e$. We note that the increase in P_{ee}, although large, is appropriate. In Table I of [28] the authors suggest a range of values that the (dimensional) parameters may assume. We use these tabulated values and the parameter definitions in Table II to compute the typical ranges for the (dimensionless) parameters P_{ee} and Γ_e. We find $0<P_{ee}<200$, and $0.056\times10^{-3}<\Gamma_e<250\times10^{-3}$, and note the typical parameter values $P_{ee}=11.0$ and $\Gamma_e=1.42\times10^{-3}$. Thus, to induce seizure-like activity in the model, we may decrease Γ_e to a value *within* the typical parameter range (e.g., $\Gamma_e=1.25\times10^{-3}$) and we must increase P_{ee} to a value *outside* the typical range (e.g., $P_{ee}=250.0$). That seizures result when we vary a parameter (here P_{ee}) to values outside its typical range is, perhaps, appropriate; we expect that seizures result from pathological changes in cortical physiology. We will discuss the relationships between model parameters and cortical physiology in a future manuscript [29].

We sought to validate the mathematical model by comparing $\tilde{h}_e$, which is proportional to the voltage observed at the cortex, with ECoG time series data recorded from a human subject during four of his seizures. To illustrate this comparison, we show in the upper (red) traces of Fig. 1 two epochs of ECoG data recorded from the subject preceding and during a seizure. We show in the lower (blue) traces numerical solutions derived from the model equations with typical and pathological (i.e., P_{ee} dramatically increased and Γ_e slightly decreased) parameter values. We scale both intervals in the observed time series by the same amount and both intervals in the simulated time series by the same amount to allow visual comparison. We note that the observed ECoG time series data and the model results agree qualitatively; the data recorded during seizure or simulated in the model with pathological values of P_{ee} and Γ_e both possess large amplitude oscillations relative to the nonseizing state with ap-

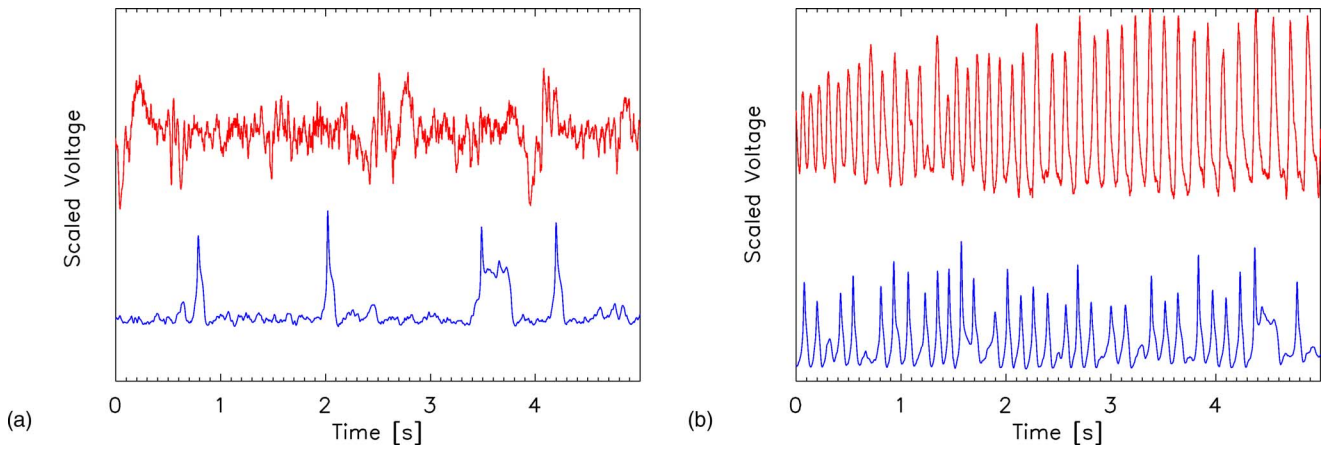

FIG. 1. (Color online) ECoG data recorded from the human cortex (upper traces in red) and data simulated in the ODE model (lower traces in blue.) (a) ECoG data recorded during the preictal state and simulated in the model with $\Gamma_e=1.42\times10^{-3}$ and $P_{ee}=11.0$. (b) ECoG data recorded during the ictal state and simulated in the model with $\Gamma_e=0.8\times10^{-3}$ and $P_{ee}=548.066$. To compute the simulated data, we employed a fourth-order Runge-Kutta method with a time step of 0.4 ms and included stochastic input. We have scaled the ECoG data in (a) and (b) by the same amount, and scaled the simulated data in (a) and (b) by the same amount to allow visual comparison.

proximately the same frequency. We quantify this result in [22] and show that the model results and ictal ECoG data agree in two important ways: the temporal frequency of oscillations, and the propagation speed of electrical activity. We conclude that the model system—derived from human cortical physiology—approximates the temporal frequency and wave speed of electrical signals in the seizing human cortex. We will compare the mathematical model with observational data from more human subjects in a future manuscript [29].

In the present work, in the interest of simplicity, we do not employ the full dimensionless SPDEs. Instead, we ignore the spatial dependence and stochastic input and consider a simpler system of dimensionless ordinary differential equations (ODEs). We state these equations and define the variables and parameters in the Appendix. We examined these dimensionless ODEs in [22] to gain insight into the complete system and found that Hopf bifurcations in the dimensionless ODEs correspond to traveling waves in the complete dimensionless SPDEs. In what follows we compute numerical solutions to the dimensionless ODEs and bifurcation diagrams using the software package AUTO (continuation and bifurcation software for ordinary differential equations) [30]. In Secs. III–V we apply a linear, differential, and filter feedback controller, respectively, to the dynamics. Here we do not attempt to apply rigorous control theory. Instead, we illustrate the effects of each controller on the bifurcations present in the dynamics. We show that all three controllers can prevent seizures [i.e., the large amplitude oscillations illustrated in Fig. 2] from occurring in the dynamics.

III. LINEAR CONTROLLER

We could attempt to control the model system through many different methods; a controller may depend on any of the 14 variables or 20 parameters, and may apply to any of the 14 differential equations in (A1). Here we employ practical considerations to constrain the form of the controller. Most of the model variables and parameters (e.g., $\tilde{\phi}_e$—the corticocortical input to excitatory cortical neurons, or N_e^α—the total number of synaptic connections from distant excitatory neurons to excitatory cortical neurons) are difficult to observe and perhaps impossible to manipulate in practice. The main observable in the model is $\tilde{h}_e=h_e/h^{\text{rest}}=h_e/(-70\text{ mV})$; this variable is proportional to the (dimensional) voltage h_e recorded in the ECoG. In practice, it is possible to manipulate cortical voltages through applied electric fields: an applied electric field polarizes the excitatory (i.e., pyramidal) neurons and thus alters the transmembrane potentials [31,32]. Following these practical considerations, we implement a controller that depends only on the variable $\tilde{h}_e$ and effects only (A1a).

We must still choose the form of the controller. In this section, we set the controller to be linear in $\tilde{h}_e$. As we mentioned in Sec. I, linear feedback controllers have been shown to ameliorate seizures in rat hippocampal brain slices *in vitro* [9]. To apply the linear controller, we redefine (A1a) as,

$$\frac{\partial\tilde{h}_e}{\partial\tilde{t}}=1-\tilde{h}_e+\Gamma_e(h_e^0-\tilde{h}_e)\tilde{I}_{ee}+\Gamma_i(h_i^0-\tilde{h}_e)\tilde{I}_{ie}+a\tilde{h}_e, \quad (1)$$

where the controller is the last term in the equation, and the parameter a represents the controller gain.

To determine how the controller effects the dynamics, we compute bifurcation diagrams of (A1) with (A1a) replaced by (1). We study bifurcation diagrams to learn which parameter changes (in Γ_e, say) dramatically alter the model dynamics. We are particularly interested in bifurcations in which the soma membrane potential changes from a relatively constant voltage to large amplitude, stable oscillations characteristic of a seizure. We compute each bifurcation diagram with all parameters fixed at the typical values (listed in Table II) except for P_{ee} and Γ_e. In each bifurcation diagram, we plot the (dimensional) variable h_e as a function of the (dimensionless) parameter Γ_e. We note that the typical values of P_{ee} and

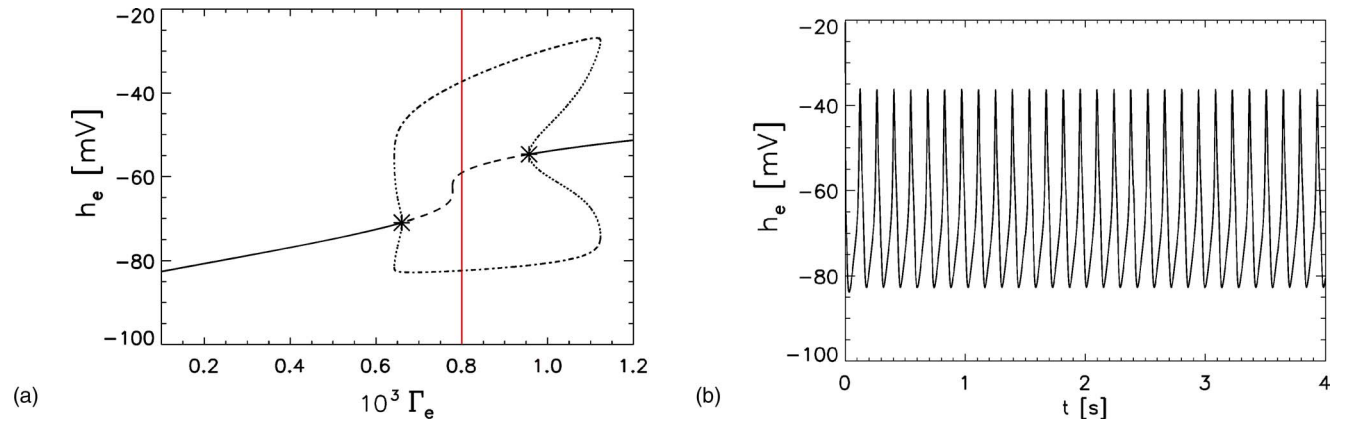

FIG. 2. (Color online) (a) Bifurcation diagram for the uncontrolled dimensionless ODEs at the pathological parameter value $P_{ee}=548.066$. The parameter Γ_e is varied and the stable (solid curves) and unstable (dashed curves) fixed points in h_e are shown. The asterisks denote two Hopf bifurcations. The dash-dot curves denote the maximum and minimum values of h_e achieved during a stable limit cycle. The dotted curves denote the maximum and minimum values of h_e achieved during an unstable limit cycle. The branch of limit cycles is born and dies in two subcritical Hopf bifurcations; two saddle-node bifurcations of limit cycles lead to large amplitude stable oscillations with sudden onset. The vertical (red) line denotes the value of Γ_e $(=0.80\times10^{-3})$ used in (b). (b) Numerical solution to the dimensionless ODEs at $P_{ee}=548.066$ and $\Gamma_e=0.80\times10^{-3}$, marked by the vertical (red) line in (a). Dimensional h_e is plotted as a function of dimensional time t. The oscillations in h_e occur at a frequency near 7.5 Hz and are stable to perturbations.

Γ_e are 11.0 and 1.42×10^{-3}, respectively. In Sec. III A we consider a pathological parameter value of $P_{ee}=548.066$ (at nearly fifty times the typical value). We will show that, without the feedback controller, the variable h_e undergoes large amplitude oscillations characteristic of a seizure at a pathological combination of parameters. However, by setting an appropriate value for the the controller gain a it is possible to abort these oscillations.

A. The pathological case of hyper-excitation $P_{ee}=548.066$

Here we set the parameter $P_{ee}=548.066$; we found in [22] that values of P_{ee} between 200 and 1000 could produce stable, large amplitude oscillations in h_e characteristic of the ictal ECoG data. In Fig. 2(a) we plot a bifurcation diagram of (A1) without the applied controller [i.e., $a=0$ in (1)]. We plot the stable and unstable fixed points in h_e as solid and dashed curves, respectively. Two Hopf bifurcations occur at $\Gamma_e=0.66\times10^{-3}$ and $\Gamma_e=0.96\times10^{-3}$, each marked by an asterisk. Both Hopf bifurcations are subcritical and give rise to unstable limit cycles. (For an introduction to Hopf bifurcations, see Sec. V.2 of [33].) These unstable limit cycles do not approximate the oscillatory activity we record in the ECoG during seizure. To induce stable, large amplitude oscillations in h_e, we adjust Γ_e until the limit cycles undergo saddle-node bifurcations at $\Gamma_e=0.64\times10^{-3}$ and $\Gamma_e=1.15\times10^{-3}$ and stabilize. We plot the maxima and minima of h_e achieved during these unstable and stable limit cycles as dotted and dot-dash curves, respectively. The model "seizes"—large amplitude oscillations occur in h_e—for values of Γ_e between the two saddle-node bifurcations of limit cycles (i.e., $0.64\times10^{-3}<\Gamma_e<1.15\times10^{-3}$). We note that the dynamics possess a subHopf/fold cycle type of bifurcation, or equivalently, the dynamics undergo elliptic bursting [14]. We define this and some other bifurcation types in Table III.

To illustrate this seizing activity—characterized by large amplitude oscillations in h_e—we plot in Fig. 2(b) a numerical solution to (A1). Here we fix the parameters to the typical values except $P_{ee}=548.066$ and $\Gamma_e=0.8\times10^{-3}$. We indicate this value of Γ_e between the two Hopf bifurcations with a vertical (red) line in Fig. 2(a). To compute the numerical solution, we use a fourth order Runge-Kutta method with a (dimensional) time step of 0.4 ms. We show in Fig. 2(b) that h_e is immediately drawn to the stable limit cycle with a maximum of −36 mV and a minimum −82 mV. These extrema correspond to the intersections of the vertical (red) line and dot-dash curves in Fig. 2(a).

Having considered the uncontrolled dynamics $(a=0.0)$, we now consider the controlled case. In Fig. 3 we show the bifurcation diagrams of (A1) with (A1a) replaced by (1) for six values of the gain a. To help visualize these results, we plot in Fig. 3(a) only the stable and unstable fixed points as solid and dashed curves, respectively, and denote the Hopf bifurcations as asterisks. We plot the results for the uncontrolled dynamics in black, and the controlled dynamics in color. We note that the bifurcation diagram for the uncontrolled dynamics is also shown in Fig. 2(a). The colors in Fig. 3 correspond to the controller gain as follows: Red $a=-0.1$, orange $a=-0.5$, light green $a=-1.0$, dark green $a=-1.67$, blue $a=-1.86$, and purple $a=-1.96$. We find that for negative gains of small magnitude the two Hopf bifurcations, originally separated by 0.28×10^{-3} in Γ_e, separate further; for $a=-1.0$ (the light green curve) the separation between the Hopf bifurcations is 0.55×10^{-3}. As we reduce a toward −1.96, the Hopf bifurcations approach one another. At $a=-1.96$ (the purple curve) no Hopf bifurcations occur and only stable fixed points remain.

To investigate the limit cycles born in the Hopf bifurcations, we plot in Fig. 3(b) the maxima and minima of h_e achieved during the stable (solid curves) and unstable (dotted curves) limit cycles. We note that the solid curves in this figure correspond to the extrema of stable limit cycles, and not to stable fixed points. The color scheme is identical to

TABLE III. Glossary of relevant bifurcations.

Bifurcation name	Definition	Illustration
Bautin bifurcation	A codimension two bifurcation in which a saddle-node of limit cycles and a subcritical Hopf bifurcation meet tangentially.	Fig. 1.13 of Ref. [14].
Hopf bifurcation	A bifurcation of a fixed point of a vector field that gives rise to a unique periodic orbit [47]. Here, when the branch of periodic orbits is stable (unstable) we call the Hopf bifurcation supercritical (subcritical).	Fig. 20.2.1 of Ref. [47]. Fig. 12 of Ref. [33].
subHopf/fold cycle	a series of bifurcations in which the rest state loses stability via a subcritical Hopf bifurcation. The unstable limit cycle born in this Hopf bifurcation stabilizes in a saddle-node bifurcation of limit cycles. The limit cycle attractor disappears via another saddle-node bifurcation of limit cycles.	Fig. 1.8 of Ref. [14].

that in Fig. 3(a); the black and color curves correspond to the uncontrolled and controlled dynamics, respectively. We denote the Hopf bifurcations with asterisks; the values of the Hopf bifurcations are identical in Figs. 3(a) and 3(b). We find that for negative gains of small magnitude both Hopf bifurcations are subcritical; the limit cycles born in these Hopf bifurcations are unstable. At $a=-0.5$ (the orange curve), the left Hopf bifurcation at $\Gamma_e=0.32\times10^{-3}$ is supercritical, and the right Hopf bifurcation at $\Gamma_e=0.83\times10^{-3}$ remains subcritical. We find, but do not show here, that this change from a subcritical Hopf bifurcation to a supercritical Hopf bifurcation results from a co-dimension two Bautin bifurcation [34].

The stabilities of the limit cycles born in the two Hopf bifurcations are preserved for more negative gains. For $a=-1.86$ (the blue curve), the two Hopf bifurcations are close in both h_e and Γ_e, and the amplitudes of the limit cycles are small. Finally, for $a=-1.96$ we find that neither the subcritical nor supercritical Hopf bifurcations remain. The transition between the state with two Hopf bifurcations (as for $a=-1.86$) and no Hopf bifurcations (as for $a=-1.96$) can be quite involved (see, for example, Fig. 4.6 of Ref. [35].) Here we are not concerned with the details of this transition. Instead, our goal is more practical and modest: the elimination of seizure-like oscillations from the dynamics. Because no Hopf bifurcations remain, we cannot plot a purple curve ($a=-1.96$) in Fig. 3(b).

Our goal in implementing the feedback controller is to eliminate large amplitude oscillations in h_e (i.e., seizures) from the model dynamics. We may use the results shown in Figs. 3(a) and 3(b) to suggest how we might achieve this goal. We found that for negative gains with small magnitude the two Hopf bifurcations separate in Γ_e. As we make the gain more negative, the two Hopf bifurcations approach and eventually disappear. Thus, for values of the gain $a\leqslant-1.96$, we expect no large amplitude oscillations in h_e. To show how the controller effects the dynamics, we compute a numerical solution to (A1) with (A1a) replaced by (1). Here we use the

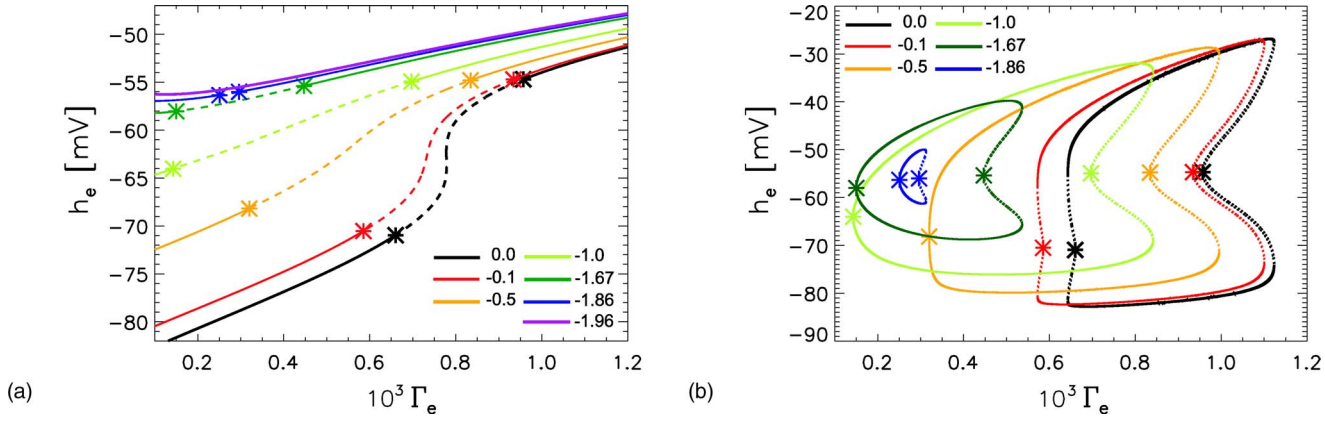

FIG. 3. (Color online) Bifurcation diagrams for the uncontrolled and controlled dynamics with pathological hyper-excitation ($P_{ee}=548.066$). (a) The parameter Γ_e is varied and the stable fixed points (solid curves), unstable fixed points (dashed curves), and Hopf bifurcations (asterisks) in h_e are shown. (b) The Hopf bifurcations (asterisks) and maxima and minima in h_e achieved during the stable (solid curves) and unstable (dotted curves) limit cycle oscillations as Γ_e is varied. The legend in both subfigures indicates the color assigned to each gain a.

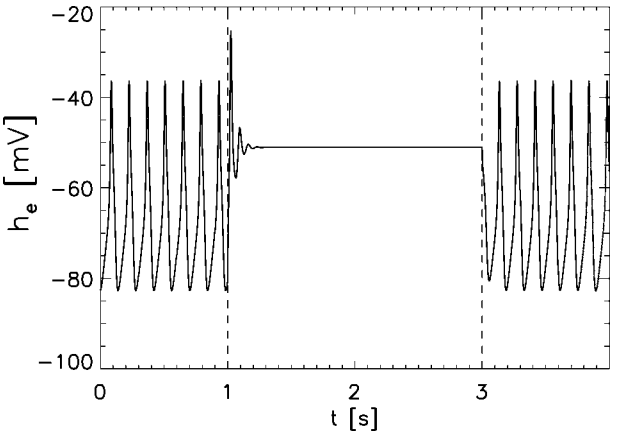

FIG. 4. Numerical solution to the dimensionless ODEs with the applied linear controller. We set parameters to the pathological values $P_{ee}=548.066$, $\Gamma_e=0.80\times10^{-3}$, and the controller gain $a=-1.96$ for 1 s$<t<$3 s, and $a=0.0$ otherwise. We plot dimensional h_e as a function of dimensional time t. At $t=1$ s (indicated by the left vertical dashed line) the active controller rapidly terminates the oscillations in h_e. At $t=3$ s (indicated by the right vertical dashed line) the controller becomes inactive and oscillations immediately develop.

same parameters ($P_{ee}=548.066$ and $\Gamma_e=0.8\times10^{-3}$) and algorithm (fourth-order Runge-Kutta with time step 0.4 ms) we used to create Fig. 2(b). In that figure, we fixed $a=0.0$. Here we set $a=-1.96$ for 1 s$<t<$3 s, and $a=0.0$ otherwise. We plot the results in Fig. 4. Initially, in the uncontrolled state, h_e undergoes large amplitude oscillations. At $t=1$ s, we turn on the controller and within 0.2 s the oscillations cease and h_e approaches a stable fixed point. When we turn off the controller at $t=3$ s, oscillations in h_e immediately develop. We note that Gluckman *et al.* find a similar seizure-after-release affect in their experimental work on rat hippocampal slices [9].

With the simple linear feedback controller, we cannot avoid the seizure-after-release phenomenon. Upon changing from the controlled (e.g., $a=-1.96$) to the uncontrolled ($a=0.0$) dynamics, the bifurcation diagram reverts to that shown in Fig. 2(a). Because we have kept the parameters $P_{ee}=548.066$ and $\Gamma_e=0.8\times10^{-3}$ fixed, h_e becomes entrained by the large amplitude, stable limit limit cycle shown in Fig. 2(b). To eliminate the seizure-after-release phenomenon, we could change one of these parameters before returning to the uncontrolled state. For example, we could increase Γ_e from 0.8×10^{-3} to 1.3×10^{-3} while the controller was active. Then, upon disabling the controller, h_e would approach a stable fixed point instead of entering a stable limit cycle. We discuss this mechanism further in Sec. VII. In the next section, we set P_{ee} to the typical value of 11.0 and show how the controller affects the model dynamics.

B. The case of normal excitation $P_{ee}=11.0$

In Sec. III A, we showed that the linear controller can eliminate oscillations in the model variable h_e. To induce these oscillations, we increased the parameter P_{ee} to nearly fifty times its normal value (i.e., we set $P_{ee}=548.066$). We now set P_{ee} to its typical value ($P_{ee}=11.0$) and show how the controller affects the normal model dynamics. This case is of practical importance; should the controller incorrectly activate during normal brain activity, it must not induce a seizure.

To start, we fix $P_{ee}=11.0$ and compute bifurcation diagrams of (A1) with (A1a) replaced by (1). In Fig. 5(a) we plot the stable (solid curves) and unstable (dashed curves) fixed points and Hopf bifurcations (asterisks) for five values of the gain a. We denote the values of a as follows: black $a=0.0$, red $a=-0.3$, orange $a=-1.0$, light-green $a=-1.96$, and purple $a=-2.2$. We note that the color scheme in Figs. 3(a) and 5(a) are different. For $a=0.0$ we find only one Hopf bifurcation at $\Gamma_e=1.21\times10^{-3}$. At $a=-0.3$ a second Hopf bifurcation appears at $\Gamma_e=2.07\times10^{-3}$. As we make the gain a more negative (to -1.0 and -1.96), we find that the two Hopf bifurcations approach in Γ_e and that neither Hopf bifurcation remains near $a=-2.2$.

The Hopf bifurcations shown in Fig. 5(a) affect the dynamics differently. To illustrate these effects, we plot in Fig.

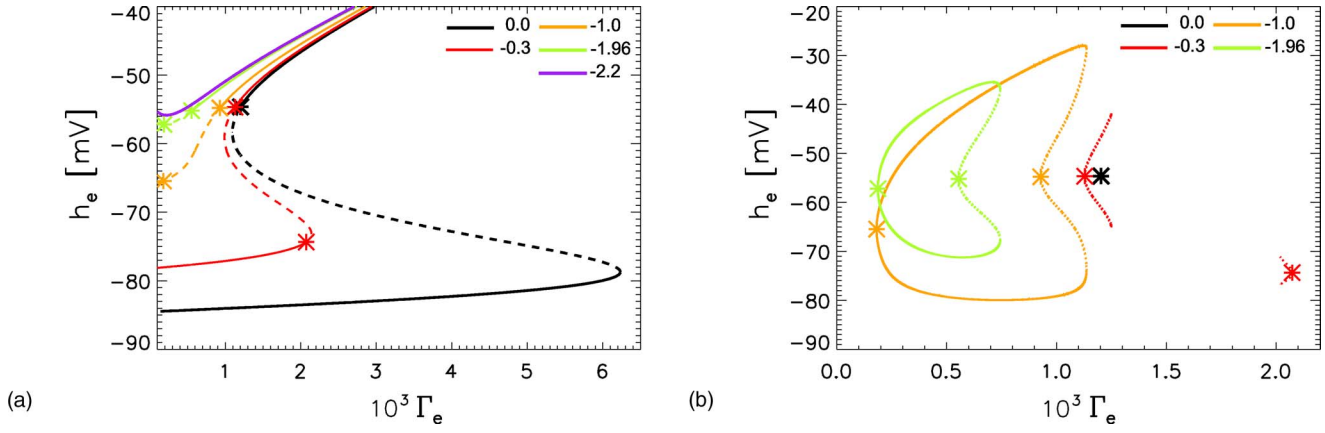

FIG. 5. (Color online) Bifurcation diagrams for the uncontrolled and controlled normal ($P_{ee}=11.0$) dynamics. (a) The parameter Γ_e is varied and the stable fixed points (solid curves), unstable fixed points (dashed curves), and Hopf bifurcations (asterisks) in h_e are shown. (b) The Hopf bifurcations (asterisks) and maxima and minima in h_e achieved during the stable (solid curves) and unstable (dotted curves) limit cycle oscillations as Γ_e is varied. The legend in both subfigures indicates the color assigned to each gain a.

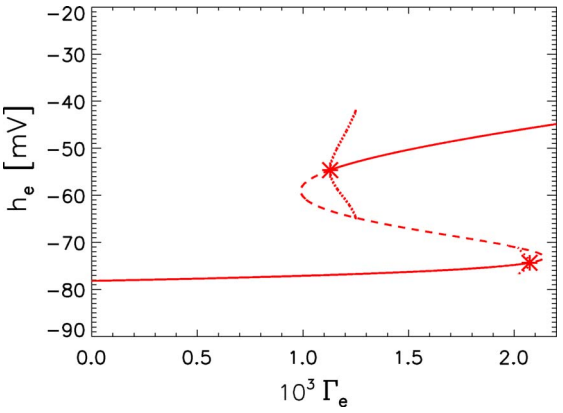

FIG. 6. (Color online) Bifurcation diagram for the controlled dimensionless ODEs at $P_{ee}=11.0$ and gain $a=-0.3$. The parameter Γ_e is varied and the stable (solid curves) and unstable (dashed curves) fixed points in h_e are shown. The asterisks denote the two Hopf bifurcations. The dotted curves denote the maximum and minimum values of h_e achieved during the unstable limit cycles. Both unstable limit cycles intersect the curve of unstable fixed points and terminate in a catastrophic event. The bifurcation diagram in this figure corresponds to red curves shown in Figs. 5(a) and 5(b).

5(b) the maxima and minima achieved by h_e during stable (solid curves) and unstable (dotted curves) limit cycles. For $a=0.0$, the Hopf bifurcation is supercritical. The unstable limit cycle born in this Hopf bifurcation increases in amplitude, and immediately intersects the branch of unstable fixed points in h_e. This transition is so abrupt that we cannot show the unstable limit cycle branch in Fig. 5(b). The resulting low amplitude, transient oscillations in h_e do not mimic the large amplitude, persistent oscillations we observe in ECoG data recorded during seizure. Thus we do not require that the controller eliminate this low amplitude, oscillatory behavior and its subsequent transition to a stable fixed point.

With this understanding of the uncontrolled ($a=0.0$) dynamics, we now consider the controlled behavior. For $a=-0.3$ we find two Hopf bifurcations, one at $\Gamma_e=1.13\times10^{-3}$—near the Hopf bifurcation found for the $a=0.0$ case—and the other at $\Gamma_e=2.07\times10^{-3}$. Both Hopf bifurcations are subcritical and produce unstable limit cycles. The limit cycles increase in amplitude and intersect the curve of unstable fixed points. To illustrate this behavior, we show in Fig. 6 the complete bifurcation diagram for gain $a=-0.3$. We note that the (red) curves in this figure correspond to the (red) curves shown in Figs. 5(a) and 5(b). The Hopf bifurcations give rise to unstable limit cycles. The amplitudes and periods of the oscillations (dotted curves) increase until the limit cycles reach the branch of unstable fixed points (dashed curves) near $\Gamma_e=1.25\times10^{-3}$ and $\Gamma_e=2.02\times10^{-3}$. At these intersections the oscillations in h_e cease, and h_e approaches a stable fixed point. Thus for small negative gains the controlled dynamics enter unstable, low amplitude limit cycles, not the high amplitude, stable limit cycles characteristic of a seizure. As we decrease the magnitude of a further we find, but do not show, that the Hopf bifurcation with a lower value of h_e undergoes a Bautin bifurcation near $a=-0.75$. Then the stable limit cycles born in the supercritical Hopf bifurcations undergo a saddle-node bifurcation of limit cycles with the unstable limit cycles born in the subcritical Hopf bifurcation. We illustrate this limit cycle behavior in Fig. 5(b) for $a=-1.0$ and $a=-1.96$. We note that with gain $a=-1.96$ the controller successfully terminates seizures in the hyper-excited ($P_{ee}=548.066$) model cortex as we show in Fig. 4. Unfortunately, the same controller and gain induces large amplitude, stable oscillations in h_e characteristic of seizures for $P_{ee}=11.0$—the typical value of subcortical excitation.

We now summarize how the Hopf bifurcations depend on the gain a and parameter Γ_e for $P_{ee}=11.0$ (the typical value.) At $a=0.0$, we find only one Hopf bifurcation at $\Gamma_e=1.21\times10^{-3}$. As we make a more negative we find a second Hopf bifurcation near $a=-0.3$. This Hopf bifurcation undergoes a Bautin bifurcation at $a=-0.75$ and the limit cycle stabilizes. The supercritical and subcritical Hopf bifurcations approach as we make a more negative and at $a=-2.15$ no Hopf bifurcations remain.

We have shown in Sec. III A that with gain $a=-1.96$, the controller eliminates seizures from the hyper-excited ($P_{ee}=548.066$) model cortex. Unfortunately, the same controller induces seizures in the model cortex with typical excitation ($P_{ee}=11.0$). We do not consider such a controller successful. Should the controller activate during near-normal activity—requiring a 40% decrease in the typical value of Γ_e—the controller may induce a seizure. To avoid this unwanted behavior, we set the gain $a=-2.4$. At this gain, we do not expect to find any Hopf bifurcations in the hyper-excited or typical dynamics. To verify this result, we compute numerical solutions to the dimensionless ODEs for $11.0<P_{ee}<1000.0$, $0.02\times10^{-3}<\Gamma_e<1.3\times10^{-3}$, and $a=0.0$, $a=-1.96$, and $a=-2.2$. We use the fourth-order Runge-Kutta method with a (dimensional) time step of 0.4 ms. We then determine the difference between the maximum and minimum achieved by the solution h_e after transient behavior has decayed. If h_e approaches a fixed point, then the maximum and minimum are nearly equal and their difference approaches zero. But, if h_e is entrained by a limit cycle then the difference between the maximum and minimum achieved by h_e is nonzero. In Fig. 7(a) we fix $a=0.0$ and plot the difference between the maximum and minimum achieved by h_e as a function of the parameters P_{ee} and Γ_e. Here white represents a 0 mV difference and purple (or black) a 50 mV difference. We find that oscillations in h_e [represented by the color (or dark) regions in Fig. 7(a)] extend over a broad range of parameter values beginning near $P_{ee}=250.0$ and $\Gamma_e=1.3\times10^{-3}$. These regions of oscillatory activity in h_e illustrate the parameter values at which the uncontrolled dimensionless ODEs "seize." In Fig. 7(b) we show the results of a similar computation with linear control with gain $a=-1.96$. The color scheme is identical to that in Fig. 7(a). We note that oscillations develop at smaller values of P_{ee} and Γ_e. We find, but do not show, that *no* seizure-like oscillations occur when we fix the gain $a=-2.4$. Thus we conclude that the linear feedback controller with gain $a=-2.4$ eliminates seizures in the hyper-excited ($P_{ee}\gg11.0$) model cortex and does not induce seizures in the model cortex with typical excitation ($P_{ee}\approx11.0$).

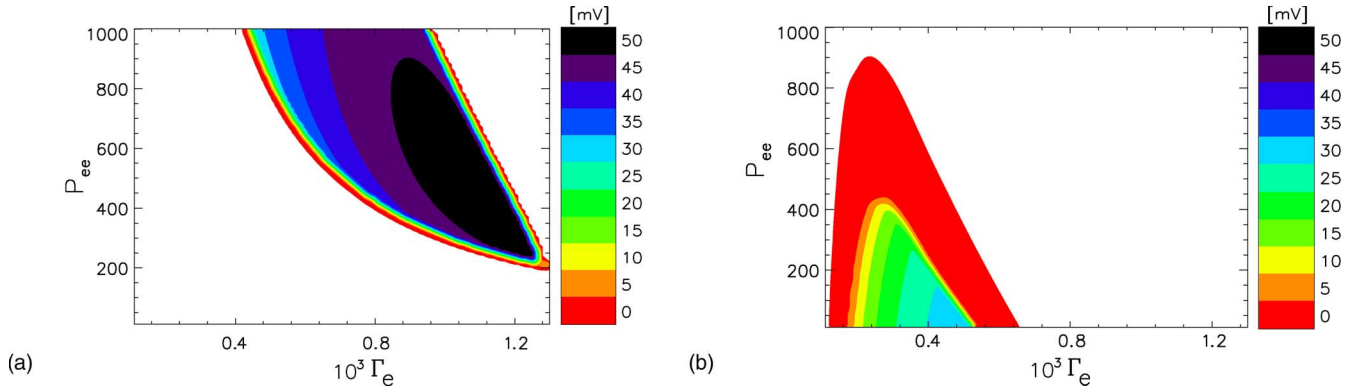

FIG. 7. (Color online) The difference between the maximum and minimum achieved by (the dimensional) h_e in solutions of the dimensionless ODEs for parameters P_{ee} and Γ_e. The difference is plotted in a linear color (gray) scale with white representing a 0 mV difference and purple (black) representing a 50 mV difference. (a) Gain $a=0.0$, the uncontrolled system. The dark region corresponds to stable "seizure" oscillations of h_e and broadens as P_{ee} is increased. (b) Gain $a=-1.96$. Stable "seizure" oscillations in h_e occur for $P_{ee} \approx 11.0$ (the typical value of P_{ee}) but at lower than the typical value of Γ_e.

IV. DIFFERENTIAL CONTROLLER

We have shown in Sec. III how we can use a feedback controller linear in h_e to halt seizures in the model cortex. Although successful in the model, the linear controller would fail in practice. To prevent tissue damage a controller should inject charge balanced currents (e.g., the biphasic pulses discussed in Sec. I) into the cortex [36]. The linear controller we discuss in Sec. III violates this important restriction. Instead, with $a=-1.96$, say, the active controller establishes a constant voltage across the cortical tissue. We show an example of this in Fig. 4. For 1 s$<t<$3 s, the controller maintains h_e at -51 mV and, therefore, establishes a constant voltage of $a\tilde{h}_e=(-1.96)\times(-51\ \text{mV})=100$ mV across the cortical tissue. This constant voltage requires a constant—not a charge balanced—continuous, current. In practice, the constant current produced by the linear controller would create unacceptable damage to cortical tissue [36].

To implement a controller that avoids damaging cortical tissue, we consider a differential controller. In [13], the authors apply a differential controller to a population of neurons interacting through global coupling. They find that, once initiated, the controller rapidly suppresses synchronous activity and decays to the noise level. We note that in Fig. 3 of Ref. [13] the controller value appears to oscillate around zero and is suggestive of a charge balanced intervention.

To apply a differential controller to (A1), we set (A1a) to:

$$\frac{\partial \tilde{h}_e[t]}{\partial \tilde{t}} = 1 - \tilde{h}_e[t] + \Gamma_e(h_e^0 - \tilde{h}_e[t])\tilde{I}_{ee}[t] + \Gamma_i(h_i^0 - \tilde{h}_e[t])\tilde{I}_{ie}[t] + b(\tilde{h}_e[t] - \tilde{h}_e[t-\tau]). \quad (2)$$

Here we explicitly state the time dependence in square brackets following each variable. The last term on the right hand side of (2) represents the controller; b denotes the controller gain, and τ the delay time. By introducing the differential controller, we change the system of ODEs in (A1) into a system of delay differential equations (DDEs). One may compute bifurcation diagrams for the DDEs (see, for example, [37]) but we will not do so here. Instead we compute numerical solutions and response diagrams to the DDEs and show how the differential controller affects the dynamics. We will show that the differential controller can stop the model dynamics from seizing with minimal net intervention.

We start by computing a numerical solution to (A1) with (A1a) replaced by (2). We fix the model parameters to the typical values except for P_{ee} and Γ_e which we set to the pathological values: $P_{ee}=548.066$ and $\Gamma_e=0.80\times10^{-3}$. We fix the delay time of the controller $\tau=20$ ms and vary the gain b as follows: For 1 s$<t<$3 s we set $b=-10.0$; otherwise $b=0.0$. We choose this value of τ from the range 18 ms$<\tau<$36 ms we have found through numerical simulation to halt seizure-like oscillations in the dynamics. We note that this range depends on the gain b. We compute the numerical solution using a fourth order Runge-Kutta method with time step of 0.4 ms and show the results in Fig. 8. We plot in the lower curve the model results for the dimensional h_e, and in the upper curve the value of the controller [i.e., the last term on the right hand side of (2)]. For $t<1$ s, the controller is inactive and the model "seizes." At $t=1$ s we activate the differential controller and its voltage quickly increases to a maximum value of 190 mV (outside of the range shown in this figure). The controller halts the seizure and, within one second, h_e approaches a fixed point. Soon afterward, the applied voltage delivered by the controller approaches zero, but continues to act weakly on the dynamics. Upon deactivating the controller at $t=3$ s, h_e drifts from the steady value and becomes entrained in the limit cycle behavior characteristic of the seizure-after-release effect.

We have shown in Fig. 8 that the differential controller with delay $\tau=20$ ms and gain $b=-10.0$ can halt seizures in the model cortex. We now consider response diagrams for the controlled dynamics with different values of the gain b. To compute each response diagram, we fix the parameters at the typical values except for $P_{ee}=548.066$ (the pathological value) and Γ_e chosen from the range $0.3\times10^{-3}<\Gamma_e<1.3\times10^{-3}$. For each value of Γ_e we solve the dimensionless DDEs using a fourth-order Runge-Kutta method with time step of 0.4 ms and total time of 1600 ms. We then compute

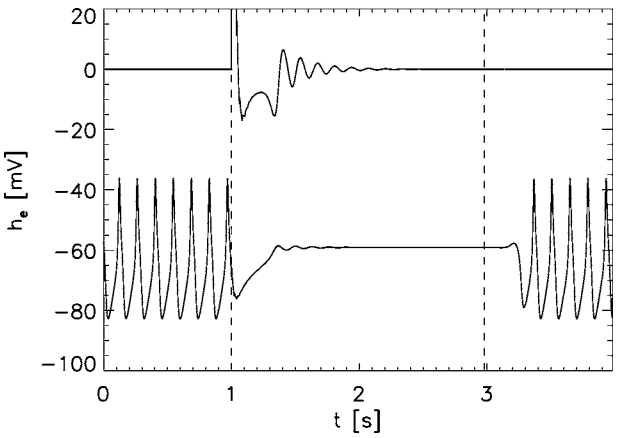

FIG. 8. Numerical solution to the dimensionless DDEs with the applied differential controller. We set parameters to the pathological values $P_{ee}=548.066$, $\Gamma_e=0.80\times10^{-3}$, and the controller gain $b=-10.0$ for 1 s$<t<$3 s, and $b=0.0$ otherwise. We plot the model results for dimensional h_e as a function of dimensional time t in the lower curve. We plot the dimensional value of the differential controller in the upper curve. At $t=1$ s (indicated by the left vertical dashed line) the active controller rapidly terminates the oscillations in h_e. At $t=3$ s (indicated by the right vertical dashed line) the controller becomes inactive and oscillations soon return.

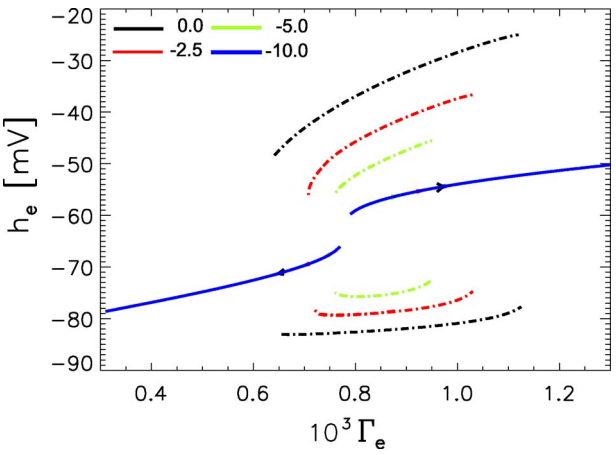

FIG. 9. (Color online) Response diagrams for the uncontrolled and differential controlled dynamics with pathological hyper-excitation ($P_{ee}=548.066$). The parameter Γ_e is varied and the stable fixed points (solid curves) and stable limit cycles (dot-dash curves) are shown. The legend indicates the color assigned to each gain b. We note that the curves of stable fixed points are nearly identical throughout the region of overlap in Γ_e.

the maximum and minimum achieved by h_e during the last 400 ms of the solution. If the dynamics approach a fixed point, then the maximum and minimum of h_e are equal. Otherwise, (e.g., if the dynamics enter a limit cycle) then the maximum and minimum are unequal. We repeat this computation for different values Γ_e that deviate from the current value by 0.01×10^{-3}. We note that the response diagram is similar to the bifurcation diagrams shown in Sec. III. An important difference is that, in the response diagrams, we can only show stable (not unstable) fixed points and limit cycles.

We show the response diagrams in Fig. 9. We plot in black the response diagram for the uncontrolled ($b=0.0$) dynamics. Where the maximum and minimum of h_e are equal, we plot black solid curves; otherwise we plot dot-dash curves. Here we find two curves of stable fixed points (the black, solid curves) and two curves of stable oscillations (the black, dot-dash curves of largest and smallest amplitudes). The stable oscillations occur for $0.65\times10^{-3}<\Gamma_e<1.15\times10^{-3}$. We note the similarity between the black curves shown in this response diagram and the stable fixed points and limit cycles shown in Fig. 2(a). As we decrease the gain b to -2.5 (the red curves) and -5.0 (the light green curves) we find that the stable oscillations—represented by the dot-dash curves—decrease in amplitude, and that the branches of stable fixed points extend over more of Γ_e. We note that the curves of stable fixed points are nearly identical in h_e throughout the regions of overlap in Γ_e. At $b=-10.0$ (the blue curves) we find no stable oscillations in the dynamics; we only find two curves of stable fixed points. We conclude that the differential controller with delay time $\tau=20$ ms and gain $b=-10.0$ can prevent seizure-like oscillations in the model cortex with pathological hyper-excitation ($P_{ee}=548.066$).

To show that the differential controller is robust to changes in the model parameters P_{ee} and Γ_e, we compute two numerical solutions to the dimensionless DDEs over the parameters $11.0<P_{ee}<1000.0$ and $0.3\times10^{-3}<\Gamma_e<1.3\times10^{-3}$. In the first solution, we fix the delay time of the differential controller $\tau=20$ ms and the gain $b=-5.0$. We then follow the same procedure and implement the same color scale as we used to create Figs. 7(a) and 7(b). We have shown the uncontrolled dynamics ($b=0.0$) in Fig. 7(a), and found that oscillatory activity (denoted by the color (or dark) regions) extends over a wide range of parameter space. In Fig. 10 we show the results for the controlled dynamics with gain $b=-5.0$. We find that oscillations remain over the same region of parameter space, although with lower amplitude.

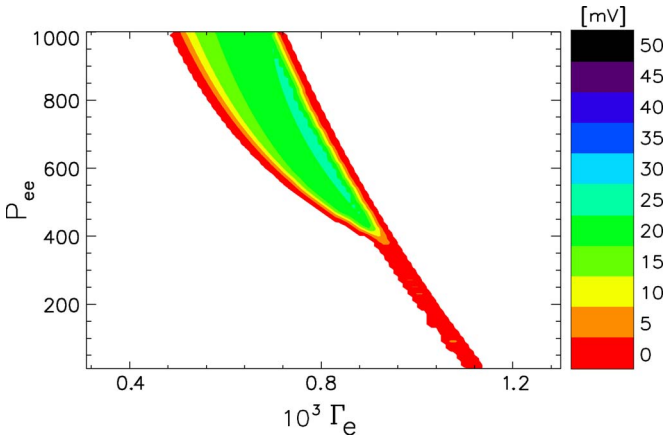

FIG. 10. (Color online) The difference between the maximum and minimum achieved by (the dimensional) h_e in solutions of the dimensionless DDEs for parameters P_{ee} and Γ_e. For the differential controller we set the delay time $\tau=20$ ms and gain $b=-5.0$. The difference is plotted in a linear color (gray) scale with white representing a 0 mV difference and purple (black) representing a 50 mV difference. The stable "seizure" oscillations of h_e broaden as P_{ee} is increased. No seizures are found over this range of parameters if $b=-10.0$.

For $b=-10.0$, we find no oscillations in h_e for any values of P_{ee} and Γ_e.

We have shown that the differential controller, like the linear controller, can halt seizures in the model cortex over a wide range of parameter values. The differential controller provides two important improvements to the linear controller. First, the applied voltage delivered by the differential controller quickly approaches zero. After h_e achieves the stable value (near −60 mV in Fig. 8) the controller may remain active with only minimal effect on the tissue. Second, the applied voltage delivered by the differential controller fluctuates around zero. For the results shown in Fig. 8, the net voltage applied by the controller is 14 mV. This voltage is much smaller—and much less damaging to cortical tissue—than that delivered by the linear controller. Here we have only considered a cursory exploration of the differential controller parameters (delay time τ and gain b.) A more detailed analysis may reveal a set of optimal parameters that further improve the differential controller over the linear controller. In the next section we consider a third type of controller: a filter controller.

V. FILTER CONTROLLER

The third strategy we employ to halt seizures in the model cortex is the application of a filter controller in $\tilde{h}_e$. In this case, the form of (A1a) becomes,

$$\frac{\partial \tilde{h}_e}{\partial \tilde{t}} = 1 - \tilde{h}_e + \Gamma_e(h_e^0 - \tilde{h}_e)\tilde{I}_{ee} + \Gamma_i(h_i^0 - \tilde{h}_e)\tilde{I}_{ie} + c\tilde{h}_{\text{filtered}}. \tag{3}$$

Here c is the controller gain, and $\tilde{h}_{\text{filtered}}$ is the result of sending $\tilde{h}_e$ through a notch filter to remove the large amplitude oscillations from the signal. The maximum attenuation of this frequency-based filter occurs at 6.75 Hz, near the natural frequency of the large amplitude oscillations that occur in $\tilde{h}_e$, which we identify with seizures. Frequencies much higher or lower than this value are not affected by the filter.

In this section, we analyze the effects of the filter controller in the same way we analyzed the differential controller in Sec. IV. Specifically, we compute numerical solutions to (A1) with (A1a) replaced by (3) for $P_{ee}=548.066$ and $P_{ee}=11.0$. We show that the filter controller can prevent seizure-like oscillations in the model dynamics for a specific value of the gain. We determine response diagrams in Γ_e for different gain values and both values of P_{ee}, and illustrate the values of P_{ee} and Γ_e at which seizure-like oscillations occur.

To begin our analysis, we compute a numerical solution to the 14 dimensionless ODEs with the applied frequency-based filter controller. We fix two parameters at the values for pathological behavior: $P_{ee}=548.066$ and $\Gamma_e=0.8\times10^{-3}$, and all other parameters at the typical values. We set the controller gain $c=0.75$ and we apply the filter controller in the SIMULINK software package of MATLAB using a positive unity feedback loop [38]. In this simulation, we turn the controller on and off at $t=1$ s and $t=3$ s, respectively.

We show the results of one of these simulations in Fig. 11. In the upper subplot we show $c\cdot h_{\text{filtered}}$—the (dimensional) output of the filter controller—which would act as the voltage input to the brain. In the lower subplot, we show the dynamics of (dimensional) h_e. We find that h_e initially decreases rapidly, as if oscillations are going to occur. However, the magnitude of the controller output steadily increases and prevents the oscillatory activity. Both the controller output and h_e reach steady values within approximately 1 s. When we turn off the controller at $t=3$ s, the seizing behavior immediately returns.

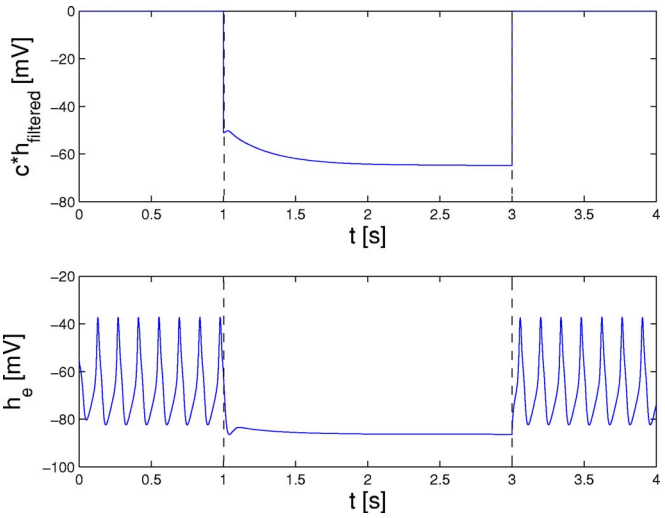

FIG. 11. (Color online) Numerical solution to the dimensionless ODEs with the applied filter controller. The parameters are set to their pathological values: $P_{ee}=548.066$ and $\Gamma_e=0.80\times10^{-3}$. The controller turns on at $t=1$ s with a gain of $c=0.75$, and it turns off at $t=3$ s. We indicate the interval of active control with two vertical dashed lines. The upper plot shows the dimensional value of the filter controller, while the lower plot displays the dimensional h_e as affected by the filter controller.

We conclude that the filter controller with gain $c=0.75$ can prevent seizure-like oscillations in the model. We now explore the effects of the controller for different values of the gain. As in Sec. IV, we create a response diagram to show the maximum and minimum values achieved by h_e after transients decay in the numerical solution. We show the response diagram for $P_{ee}=548.066$ and $0.2\times10^{-3}<\Gamma_e<1.6\times10^{-3}$ in Fig. 12. As we increase the controller gain from $c=0.15$ (the red curves) to $c=0.3$ (the green curves), the lower branch of stable fixed points decreases in h_e, while the upper branch remains nearly the same for all values of the gain. We also find that the maximum values achieved by the stable oscillations decrease as the gain increases, while the minimum values remain nearly unaffected. For $c=0.75$, we find two branches of stable fixed points and no stable oscillations. Thus we conclude that the filter controller with $c=0.75$ successfully prevents large amplitude, seizure-like oscillations from occurring in the dynamics.

Having shown that the filter controller can prevent seizure-like oscillations in the hyper-excited model ($P_{ee}=548.066$), we also consider the dynamics of the controlled system when P_{ee} is at a typical value ($P_{ee}=11.0$). We find (but do not show) that no stable oscillations occur for any value of the gain. Therefore, we conclude that the filter con-

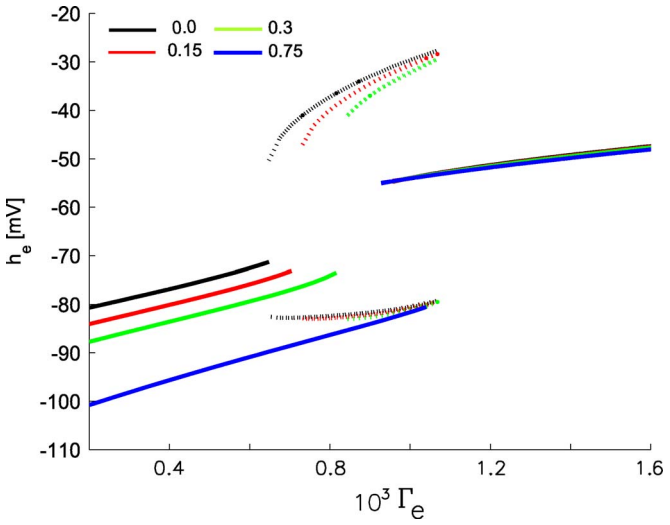

FIG. 12. (Color online) Response diagrams for the uncontrolled and filter controlled dynamics with pathological hyper-excitation (P_{ee}=548.066). In these plots, we vary Γ_e and determine the stable fixed points (solid curves) and stable limit cycles (dotted curves) at each value. The legend indicates the color assigned to each gain c.

troller does not induce seizure-like oscillations when the parameters are in the normal operating ranges.

Finally, to characterize how the values of P_{ee} and Γ_e affect the controlled system, we compute a difference plot in the same way we computed those shown in Fig. 7 for the linear controller and Fig. 10 for the differential controller. In Fig. 13 we show the difference between the maximum and minimum values achieved by h_e for different values of P_{ee} and Γ_e for the controlled dynamics with gain c=0.6. We use the same color scheme as that applied in the previous difference plots. Comparing this figure to the uncontrolled system

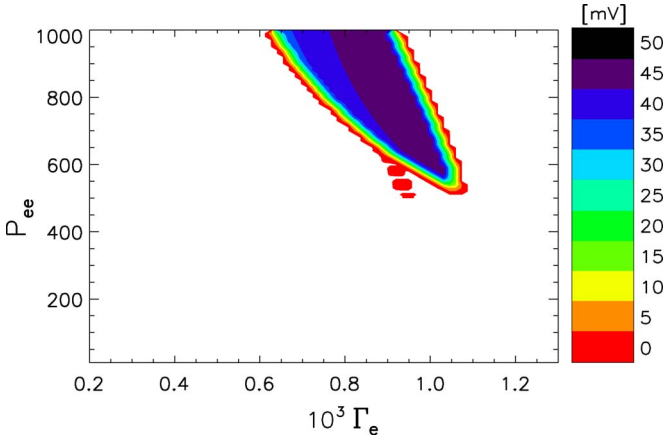

FIG. 13. (Color online) The difference between the maximum and minimum achieved by (the dimensional) h_e in solutions of the dimensionless ODEs with applied filter control for parameters P_{ee} and Γ_e. The difference is plotted in a linear color (gray) scale with white representing a 0 mV difference and purple (black) representing a 50 mV difference. Gain c=0.6 for the filter controller. The dark region corresponds to stable "seizure" oscillations of h_e and broadens as P_{ee} is increased. An increase in c to 0.75 eliminates the seizure region entirely over this range of parameters.

[Fig. 7(a)], we find that the region of oscillatory behavior has the same shape in both cases. However, as we increase the gain of the filter controller, we find that the region of oscillations shrinks and moves toward higher values of P_{ee}. When the gain is high enough (c=0.75) we find no oscillatory behavior in h_e.

We have shown that the filter controller can halt seizure-like oscillations in the model cortex. This method may not be useful in practice, however, because it relies on sending a voltage to the brain that constantly increases over a few seconds. This could damage brain tissue—the input current is not charge balanced. On the other hand, the signal from the controller, $c \cdot h_{\text{filtered}}$, changes gradually and has a relatively low maximum magnitude. The highest magnitude achieved by the filter controller is roughly 60 mV, while the differential controller (shown in Fig. 8) undergoes a large increase to 190 mV at its onset. We note that in the examples considered here the effect of the filter controller is to hyperpolarize h_e. As suggested by an anonymous referee, the controller removes the dominant seizure frequency from h_e and inputs the residual to the dynamics; in this case a constant, negative voltage—as shown in the top of Fig. 11—dominates the residual input. We find, but do not show, that for negative gains of large magnitude (e.g., c=−5) the filter controller also successfully halts seizure-like oscillations in the model dynamics.

VI. CONTROL OF STOCHASTIC PARTIAL DIFFERENTIAL EQUATIONS

We have shown in Secs. III–V how three different controllers can terminate seizure-like oscillations of the model equations (A1). We chose this system of ODEs as a simplification of the complete mathematical model described in [22]. In this section we include the spatial dependence and stochastic input of the model and apply the differential controller (described in Sec. IV) to the complete system. Specifically, we replace (A1) with the system of stochastic partial differential equations (SPDEs):

$$\frac{\partial \tilde{h}_e}{\partial \tilde{t}} = 1 - \tilde{h}_e + \Gamma_e(h_e^0 - \tilde{h}_e)\tilde{I}_{ee} + \Gamma_i(h_i^0 - \tilde{h}_e)\tilde{I}_{ie} + b(\tilde{h}_e[t] - \tilde{h}_e[t-\tau]) \tag{4a}$$

$$\frac{\partial \tilde{h}_i}{\partial \tilde{t}} = 1 - \tilde{h}_i + \Gamma_e(h_e^0 - \tilde{h}_i)\tilde{I}_{ei} + \Gamma_i(h_i^0 - \tilde{h}_i)\tilde{I}_{ii} \tag{4b}$$

$$\frac{\partial \tilde{I}_{ee}}{\partial \tilde{t}} = \tilde{J}_{ee} \tag{4c}$$

$$\frac{\partial \tilde{J}_{ee}}{\partial \tilde{t}} = -2T_e\tilde{J}_{ee} - T_e^2\tilde{I}_{ee} + T_e^2(N_e^\beta \tilde{S}_e[\tilde{h}_e] + \tilde{\phi}_e + P_{ee} + \tilde{\Gamma}_1) \tag{4d}$$

$$\frac{\partial \tilde{I}_{ei}}{\partial \tilde{t}} = \tilde{J}_{ei} \tag{4e}$$

$$\frac{\partial \tilde{J}_{ei}}{\partial \tilde{t}} = -2T_e\tilde{J}_{ei} - T_e^2\tilde{I}_{ei} + T_e^2(N_e^\beta \tilde{S}_e[\tilde{h}_e] + \tilde{\phi}_i + P_{ei} + \tilde{\Gamma}_2) \tag{4f}$$

$$\frac{\partial \tilde{I}_{ie}}{\partial \tilde{t}} = \tilde{J}_{ie} \tag{4g}$$

$$\frac{\partial \tilde{J}_{ie}}{\partial \tilde{t}} = -2T_i\tilde{J}_{ie} - T_i^2\tilde{I}_{ie} + T_i^2(N_i^\beta \tilde{S}_i[\tilde{h}_i] + P_{ie} + \tilde{\Gamma}_3) \tag{4h}$$

$$\frac{\partial \tilde{I}_{ii}}{\partial \tilde{t}} = \tilde{J}_{ii} \tag{4i}$$

$$\frac{\partial \tilde{J}_{ii}}{\partial \tilde{t}} = -2T_i\tilde{J}_{ii} - T_i^2\tilde{I}_{ii} + T_i^2(N_i^\beta \tilde{S}_i[\tilde{h}_i] + P_{ii} + \tilde{\Gamma}_4) \tag{4j}$$

$$\frac{\partial \tilde{\phi}_e}{\partial \tilde{t}} = \tilde{\psi}_e \tag{4k}$$

$$\frac{\partial \tilde{\psi}_e}{\partial \tilde{t}} = \frac{\partial^2 \tilde{\phi}_e}{\partial \tilde{x}^2} - 2\lambda_e\tilde{\psi}_e - \lambda_e^2\tilde{\phi}_e + \lambda_e N_e^\alpha \frac{\partial \tilde{S}_e[\tilde{h}_e]}{\partial \tilde{t}} + \lambda_e^2 N_e^\alpha \tilde{S}_e[\tilde{h}_e] \tag{4l}$$

$$\frac{\partial \tilde{\phi}_i}{\partial \tilde{t}} = \tilde{\psi}_i \tag{4m}$$

$$\frac{\partial \tilde{\psi}_i}{\partial \tilde{t}} = \frac{\partial^2 \tilde{\phi}_i}{\partial \tilde{x}^2} - 2\lambda_i\tilde{\psi}_i - \lambda_i^2\tilde{\phi}_i + \lambda_i N_i^\alpha \frac{\partial \tilde{S}_e[\tilde{h}_e]}{\partial \tilde{t}} + \lambda_i^2 N_i^\alpha \tilde{S}_e[\tilde{h}_e]. \tag{4n}$$

Here, the (dimensionless) variables and parameters are now functions of (dimensionless) time $\tilde{t}$ and (dimensionless) space $\tilde{x}$, where $\tilde{x}=x/(\tau v)$ in terms of the dimensional variables of [21]. The complete system of SPDEs in (4) differs from the simplified system of ODEs in (A1) in three ways. First, we include the differential controller (with gain b and delay time τ) as the last term on the right hand side of (4a). Second, we introduce the second-order spatial derivatives as the first terms on the right hand sides of (4l) and (4n). Third, we include the dimensionless stochastic input terms:

$$\tilde{\Gamma}_1 = \alpha_{ee}\sqrt{P_{ee}}\xi_1[\tilde{x},\tilde{t}] \tag{5a}$$

$$\tilde{\Gamma}_2 = \alpha_{ei}\sqrt{P_{ei}}\xi_2[\tilde{x},\tilde{t}] \tag{5b}$$

$$\tilde{\Gamma}_3 = \alpha_{ie}\sqrt{P_{ie}}\xi_3[\tilde{x},\tilde{t}] \tag{5c}$$

$$\tilde{\Gamma}_4 = \alpha_{ii}\sqrt{P_{ii}}\xi_4[\tilde{x},\tilde{t}], \tag{5d}$$

in (4d), (4f), (4h), and (4j). These terms represent the noise that arises from subcortical inputs to the cortex. Here the ξ_k are Gaussian distributed white noise sources with zero mean and δ-function correlations. In numerical simulations we approximate ξ_k as,

$$\xi_k[\tilde{x},\tilde{t}] = \frac{R(m,n)}{\sqrt{\Delta\tilde{x}\Delta\tilde{t}}}, \tag{6}$$

where $\tilde{x}=m\Delta\tilde{x}$ and $\tilde{t}=n\Delta\tilde{t}$ (m,n integers) specify space and time coordinates on a lattice with (dimensionless) grid spacings, $\Delta\tilde{x}$ and $\Delta\tilde{t}$, respectively. We set $\alpha_{ee}=\alpha_{ei}=\alpha_{ie}=\alpha_{ii}=\alpha$ as in the stochastic simulations of the spatioadiabatic one-dimensional cortex in [21,22]. In the simulation that follows, we fix $\alpha=0.001$.

We now compute a numerical solution to (4). To do so, we fix all of the parameters at the typical values except for Γ_e and P_{ee}. We set $\Gamma_e=0.8\times10^{-3}$ uniform in space, and P_{ee} Gaussian in space with a maximum of 548.066 at $x=350$ mm, a full width at half maximum of 46 mm, and a minimum of 11.0. We choose this Gaussian profile for P_{ee} to construct a region of hyper-excitation localized in space; we think of this region as the location of seizure manifestation on the cortex. We set the controller delay time to $\tau=20$ ms and the gain b to be Gaussian in space with a minimum b_0 at $x=350$ mm, a full width at half minimum of 46 mm, and a maximum of $b=0.0$. We vary the minimum of the gain b_0 as follows: $b_0=-10.0$ for 500 ms$<t<$1000 ms, and $b_0=0.0$ otherwise. We note that the controller is only active for 500 ms$<t<$1000 ms. We compute numerical solutions to (4) using the Euler-Maruyama algorithm with fixed steps in space and time, 14 and 0.1 ms, respectively, and boundary conditions periodic in space [39].

We show the results in Fig. 14. Here we plot the (dimensional) value of h_e in linear gray scale, with white representing -100 mV and black representing 0.0 mV, as a function of (dimensional) space and time. For $t<500$ ms, we find that waves—represented by the dark ridges—emanate from the region of hyper-excitation at $x=350$ mm. These waves travel outward to less excited ($P_{ee}\approx11.0$) spatial regions and there decay. We showed in [22] that the speed and temporal frequency of these waves agree with observed ECoG data recorded from a human subject during seizure. At $t=500$ ms, we activate the controller. Almost immediately, the traveling wave solutions cease and h_e fluctuates around a stable value at each point in space. During the time interval of active control, the mean and standard deviation of h_e at $x=350$ mm are -70 and 2 mV, respectively. We note that at the typical parameter values ($\Gamma_e=1.42\times10^{-3}$ and $P_{ee}=11.0$) we find in numerical solutions to (4) with $b=0.0$ a mean and standard deviation of h_e of -51.9 and 0.6 mV, respectively. At $t=1000$ ms, we deactivate the controller and the traveling wave solutions reappear.

We conclude that the differential controller can abort seizures in the complete system of SPDEs (4). Here we only consider one instance of the dimensionless SPDEs, with P_{ee} and b both Gaussian in space. We find that the controller halts the traveling waves in h_e characteristic of a seizure. Like the controlled ODEs, the controlled SPDEs exhibit the seizure-after-release effect. Upon deactivation of the controller at $t=1000$ ms, the traveling wave solutions develop. To

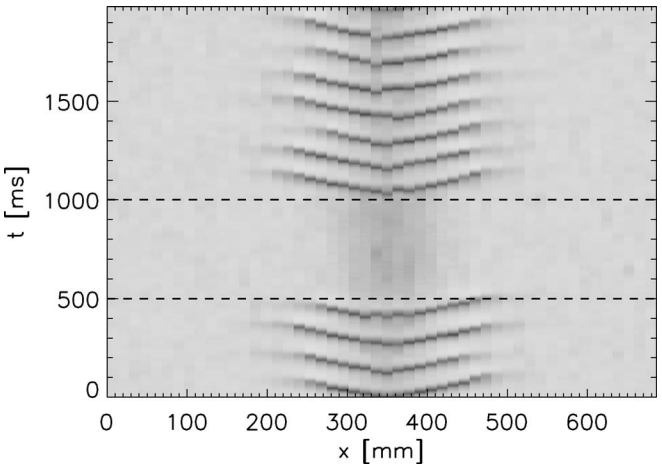

FIG. 14. Numerical solution to the controlled dimensionless SPDEs with parameters: $\Gamma_e=0.8\times10^{-3}$, $\alpha=0.001$, and P_{ee} and b both Gaussian functions in space, each with an extremum at $x=350$ mm and a full width at half the extremum at 46 mm. The boundary conditions are in periodic in space. Space (in mm) and time (in ms) are plotted along the horizontal and vertical axes, respectively. The value of h_e is plotted in linear grayscale with $h_e=-100$ mV in white and $h_e=0.0$ mV in black. For $t<500$ ms, waves in h_e travel outward from the region of hyper-excitation near $x=350$ mm. At $t=500$ ms (indicated by a horizontal dashed line) we activate the differential controller—we set the minimum of the gain $b_0=-10.0$ and $\tau=20$ ms. The traveling waves in h_e cease until we deactivate the controller at $t=1000$ ms (indicated by a horizontal dashed line).

avoid this effect, we suggest that a more effective controller would manipulate an additional model parameter (e.g., increase Γ_e or decrease P_{ee}) before returning to the uncontrolled $b=0.0$ state.

An analysis of the SPDEs model more relevant to observational data would include a second spatial dimension. We have found (but do not show here) that for pathological parameter values of Γ_e and P_{ee} complicated spatial patterns (e.g., spirals) may form on the two-dimensional cortical plane. We have not attempted to compare these patterns with human ECoG data; to do so would require high density spatial sampling, such as optical imaging [40]. We anticipate that the controller schemes we consider here in one spatial dimension will succeed in two spatial dimensions as well.

VII. DISCUSSION

In this work, we considered a mathematical model of human cortical electrical activity. We showed how to make the model seize, and explored three methods for controlling the large amplitude, stable "seizure" oscillations in h_e. In Sec. III we applied a linear feedback controller to the model. We showed that with a gain of $a=-2.4$ the controller prevented seizures in the hyper-excited cortex ($P_{ee}\gg11.0$) and did not induce seizures in the typical cortex ($P_{ee}\approx11.0$.) Unfortunately, the linear controller failed in one important aspect of practical importance: the linear controller established a large net voltage across the cortex. To correct for this, we applied a differential controller to the model in Sec. IV. We showed that the differential controller can also halt seizures in the hyper-excited cortex and established only a small net voltage across the cortex. In Sec. V we applied a filter controller to the model dynamics. We found that this controller could halt seizures in the hyper-excited cortex and delivered a maximum voltage smaller in magnitude than that delivered by the differential controller. Finally, in Sec. VI we applied the differential controller to an example of the SPDEs. We showed that the controller can abort the traveling waves of excitation characteristic of seizures in the complete model.

In our discussions of Figs. 4, 8, and 11 we noted that upon cessation of the linear and differential controllers seizures soon developed. Therefore, the controller must continually act on the system to prevent the seizure from occurring. Such a controller would require a large power source. Moreover prolonged voltage control, even at low voltages, may damage the cortex [36]. To prevent (not just temporarily halt) a seizure, the controller must affect another model parameter. We showed in [22] that seizures occur in the model after a change in two parameters: P_{ee} and Γ_e. A successful strategy employing linear feedback control would allow the controller to also effect P_{ee}. To prevent a seizure, this new controller would first activate the voltage feedback controller and then slowly decrease P_{ee} until the dynamics reach a safe range outside of the subHopf/fold cycle bifurcation. This controller operating on h_e and P_{ee} would avoid the seizure-after-release effect.

These results lead us to propose an implantable seizure control device acting via two mechanisms. Immediately after seizure initiation, a voltage controller activates and temporarily halts the seizure. A chemical controller then activates and injects a drug either systemically or locally, into the brain. After the drugs take effect—perhaps a few minutes later—the voltage controller may be relaxed without inducing a seizure. We suggest that the effect of the voltage controller is an immediate arrest of the seizure, while the effect of the second, chemical controller is prevention of seizure-after-release. If the action of the chemical controller is temporary (i.e., it produces a temporary decrease in P_{ee}) then we expect the seizure to return as the effect of the drugs diminishes. To prevent the seizure the drugs must create a stable, semi-permanent change (i.e., a semi-permanent decrease in P_{ee}) such as the post-ictal cortical state. We will discuss the relationships between chemical interventions and the model parameters in a future manuscript [29].

We have not considered several important practical issues in developing BES methods. First, to apply responsive cortical BES one must detect a seizure. An optimal seizure detection algorithm is an important and unresolved research topic [41,42]. Second, the dimensionless ODEs are not an exact model of human cortical electrical activity. Finding an adequate controller for the model is, of course, not enough to justify clinical experiments. By changing the model parameters, one may develop a mesoscale model for electrical activity in, say, rat cortex where model results may be more readily tested [43]. Finally, we have not considered whether the electrical stimulation induced by the three controllers will damage cortical tissue. To do so approximately, we assume: a uniform cortical conductivity of 0.15 s/m [44], a

cortical thickness of 5 mm, an applied voltage of 100 mV, and a pulse duration—here, half the oscillation period—of 0.1 s. Using these assumptions, we calculate an estimate of the charge per phase injected by the controller of 7.5 μC. If we further assume that area of the stimulation electrode is 1 cm^2 (large enough to cover many cortical columns) then the charge density—defined as the charge per phase divided by the electrode surface area—is 7.5 $\mu C/cm^2$. This combination of charge per phase and charge density satisfies stimulation induced safety limits (see Fig. 9.1 of Ref. [36] and see [45].) To confirm this result a more detailed analysis, perhaps involving multiple stimulation electrodes and a model of the human brain, is required [46].

Many exciting prospects exist for future epilepsy treatments. As seizure detection and localization algorithms improve, therapies may become more localized in both space and time. Similarly, as brain models improve, more effective and robust therapies may be developed. In time, mathematical models may aid in developing an implanted microprocessor that would detect cortical seizures and deliver electrical impulses and drug therapies to specific brain regions.

APPENDIX: MODEL EQUATIONS

We state the dimensionless ODEs in (A1a)–(A1n). The system consists of fourteen, first order ODEs, one for each of the variables ($\tilde{h}_e$, $\tilde{h}_i$, $\tilde{I}_{ee}$, $\tilde{J}_{ee}$, $\tilde{I}_{ei}$, $\tilde{J}_{ei}$, $\tilde{I}_{ie}$, $\tilde{J}_{ie}$, $\tilde{I}_{ii}$, $\tilde{J}_{ii}$, $\tilde{\phi}_e$, $\tilde{\psi}_e$, $\tilde{\phi}_i$, and $\tilde{\psi}_i$). We define the 14 variables in Table I and the 20 parameters in Table II in terms of dimensional quantities. The interested reader may learn more about the model in [22] and references therein.

$$\frac{\partial \tilde{h}_e}{\partial \tilde{t}} = 1 - \tilde{h}_e + \Gamma_e(h_e^0 - \tilde{h}_e)\tilde{I}_{ee} + \Gamma_i(h_i^0 - \tilde{h}_e)\tilde{I}_{ie} \quad \text{(A1a)}$$

$$\frac{\partial \tilde{h}_i}{\partial \tilde{t}} = 1 - \tilde{h}_i + \Gamma_e(h_e^0 - \tilde{h}_i)\tilde{I}_{ei} + \Gamma_i(h_i^0 - \tilde{h}_i)\tilde{I}_{ii} \quad \text{(A1b)}$$

$$\frac{\partial \tilde{I}_{ee}}{\partial \tilde{t}} = \tilde{J}_{ee} \quad \text{(A1c)}$$

$$\frac{\partial \tilde{J}_{ee}}{\partial \tilde{t}} = -2T_e\tilde{J}_{ee} - T_e^2\tilde{I}_{ee} + T_e^2(N_e^\beta \tilde{S}_e[\tilde{h}_e] + \tilde{\phi}_e + P_{ee}) \quad \text{(A1d)}$$

$$\frac{\partial \tilde{I}_{ei}}{\partial \tilde{t}} = \tilde{J}_{ei} \quad \text{(A1e)}$$

$$\frac{\partial \tilde{J}_{ei}}{\partial \tilde{t}} = -2T_e\tilde{J}_{ei} - T_e^2\tilde{I}_{ei} + T_e^2(N_e^\beta \tilde{S}_e[\tilde{h}_e] + \tilde{\phi}_i + P_{ei}) \quad \text{(A1f)}$$

$$\frac{\partial \tilde{I}_{ie}}{\partial \tilde{t}} = \tilde{J}_{ie} \quad \text{(A1g)}$$

$$\frac{\partial \tilde{J}_{ie}}{\partial \tilde{t}} = -2T_i\tilde{J}_{ie} - T_i^2\tilde{I}_{ie} + T_i^2(N_i^\beta \tilde{S}_i[\tilde{h}_i] + P_{ie}) \quad \text{(A1h)}$$

$$\frac{\partial \tilde{I}_{ii}}{\partial \tilde{t}} = \tilde{J}_{ii} \quad \text{(A1i)}$$

$$\frac{\partial \tilde{J}_{ii}}{\partial \tilde{t}} = -2T_i\tilde{J}_{ii} - T_i^2\tilde{I}_{ii} + T_i^2(N_i^\beta \tilde{S}_i[\tilde{h}_i] + P_{ii}) \quad \text{(A1j)}$$

$$\frac{\partial \tilde{\phi}_e}{\partial \tilde{t}} = \tilde{\psi}_e \quad \text{(A1k)}$$

$$\frac{\partial \tilde{\psi}_e}{\partial \tilde{t}} = -2\lambda_e\tilde{\psi}_e - \lambda_e^2\tilde{\phi}_e + \lambda_e N_e^\alpha \frac{\partial \tilde{S}_e[\tilde{h}_e]}{\partial \tilde{t}} + \lambda_e^2 N_e^\alpha \tilde{S}_e[\tilde{h}_e] \quad \text{(A1l)}$$

$$\frac{\partial \tilde{\phi}_i}{\partial \tilde{t}} = \tilde{\psi}_i \quad \text{(A1m)}$$

$$\frac{\partial \tilde{\psi}_i}{\partial \tilde{t}} = -2\lambda_i\tilde{\psi}_i - \lambda_i^2\tilde{\phi}_i + \lambda_i N_i^\alpha \frac{\partial \tilde{S}_e[\tilde{h}_e]}{\partial \tilde{t}} + \lambda_i^2 N_i^\alpha \tilde{S}_e[\tilde{h}_e]. \quad \text{(A1n)}$$

Here $\tilde{S}_e[\tilde{h}_e]$ and $\tilde{S}_i[\tilde{h}_i]$ are the dimensionless sigmoid transfer functions:

$$\tilde{S}_e[\tilde{h}_e] = \frac{1}{1 + \exp[-\tilde{g}_e(\tilde{h}_e - \tilde{\theta}_e)]} \quad \text{(A2a)}$$

$$\tilde{S}_i[\tilde{h}_i] = \frac{1}{1 + \exp[-\tilde{g}_i(\tilde{h}_i - \tilde{\theta}_i)]}. \quad \text{(A2b)}$$

[1] *Epilepsy: An introduction* (2005), URL http://www.epilepsyfoundation.org/

[2] W. H. Theodore and R. S. Fisher, Lancet Neurol. **3**, 111 (2004).

[3] R. P. Lesser, S. H. Kim, L. Beyderman, D. L. Miglioretti, W. R. S. Webber, M. Bare, B. Cysyk, G. Krauss, and B. Gordon, Neurology **53**, 2073 (1999).

[4] G. K. Motamedi, R. P. Lesser, D. L. Miglioretti, Y. Mizuno-Matsumoto, B. Gordon, W. R. S. Webber, D. C. Jackson, J. P. Sepkuty, and N. E. Crone, Epilepsia **43**, 836 (2002).

[5] E. H. Kossoff, E. K. Ritzl, J. M. Politsky, A. M. Murro, J. R. Smith, R. B. Duckrow, D. D. Spencer, and G. K. Bergey,

Epilepsia **45**, 1560 (2004).
[6] M. Kinoshita, A. Ikeda, R. Matsumoto, T. Begum, K. Usui, J. Yamamoto, M. Matsuhashi, M. Takayama, N. Mikuni, J. Takahashi *et al.*, Epilepsia **45**, 787 (2004).
[7] S. A. Chkhenkeli, M. Sramka, G. S. Lortkipanidze, T. N. Rakviashvili, E. S. Bregvadze, G. E. Magalashvili, T. S. Gagoshidze, and I. S. Chkhenkeli, Clin. Neurol. Neurosurg. **106**, 318 (2004).
[8] B. J. Gluckman, E. J. Neel, T. I. Netoff, W. L. Ditto, M. L. Spano, and S. J. Schiff, J. Neurophysiol. **76**, 4202 (1996).
[9] B. J. Gluckman, H. Nguyen, S. L. Weinstein, and S. J. Schiff, J. Neurosci. **21**, 590 (2001).
[10] R. D. Traub, R. K. Wong, R. Miles, and H. Michelson, J. Neurophysiol. **66**, 635 (1991).
[11] R. D. Traub, C. Borck, S. B. Colling, and J. G. R. Jefferys, Epilepsia **37**, 879 (1996).
[12] P. A. Tass, Prog. Theor. Phys. Suppl. **139**, 301 (2000).
[13] M. Rosenblum and A. Pikovsky, Phys. Rev. E **70**, 041904 (2004).
[14] E. M. Izhikevich, SIAM Rev. **43**, 315 (2001).
[15] H. Markram, Nat. Rev. Neurosci. **7**, 153 (2006).
[16] R. B. Traub, D. Contreras, M. O. Cunningham, H. Murray, F. E. N. LeBeau, A. Roopun, A. Bibbig, W. B. Wilent, M. J. Higley, and M. A. Whittington, J. Neurophysiol. **93**, 2194 (2005).
[17] H. R. Wilson and J. D. Cowan, Biophys. J. **12**, 1 (1972).
[18] W. J. Freeman, Exp. Neurol. **10**, 525 (1964).
[19] D. T. J. Liley, P. J. Cadusch, and J. J. Wright, Neurocomputing **26–27**, 795 (1999).
[20] M. L. Steyn-Ross, D. A. Steyn-Ross, J. W. Sleigh, and D. T. J. Liley, Phys. Rev. E **60**, 7299 (1999).
[21] M. L. Steyn-Ross, D. A. Steyn-Ross, J. W. Sleigh, and D. R. Whiting, Phys. Rev. E **68**, 021902 (2003).
[22] M. A. Kramer, H. E. Kirsch, and A. J. Szeri, J. R. Soc., Interface **2**, 113 (2005).
[23] D. T. J. Liley, P. J. Cadusch, and M. P. Dafilis, Network Comput. Neural Syst. **13**, 67 (2002).
[24] V. Mountcastle, Brain **120**, 701 (1997).
[25] E. Niedermeyer and F. L. DaSilva, eds., *Electroencephalography: Basic Principles, Clinical Applications, and Related Fields* (Lippincott Williams and Wilkins, New York, 1999).
[26] M. A. Dichter and G. F. Ayala, Science **237**, 157 (1987).
[27] F. L. da Silva, W. Blanes, S. N. Kalitzin, J. Parra, P. Suffczynski, and D. N. Velis, Epilepsia **44**, 72 (2003).
[28] I. Bojak and D. T. J. Liley, Phys. Rev. E **71**, 041902 (2005).
[29] M. A. Kramer, A. J. Szeri, J. W. Sleigh, and H. E. Kirsch (in preparation).
[30] E. Doedel, R. Paffenroth, A. Champneys, T. Fairgrieve, Y. A. Kuznetsov, B. Sandstede, and X. Wang, AUTO 2000: *Continuation and bifurcation software for ordinary differential equations (with homcont)*, http://sourceforge.net/projects/auto2000/ (2000).
[31] C. Y. Chan and C. Nicholson, J. Physiol. (London) **371**, 89 (1986).
[32] D. Tranchina and C. Nicholson, Biophys. J. **50**, 1139 (1986).
[33] J. D. Crawford, Rev. Mod. Phys. **63**, 991 (1991).
[34] M. A. Kramer, Ph.D. thesis, University of California, Berkeley (2005).
[35] M. Golubitsky and W. F. Langford, J. Diff. Eqns. **41**, 375 (1980).
[36] W. F. Agnew, D. B. McCreery, T. G. H. Yuen, and L. A. Bullara, in *Neural Prostheses: Fundamental Studies*, edited by W. F. Agnew and D. B. McCreery (Prentice Hall, Englewood Cliffs, New Jersey, 1990), Chap. 9, pp. 226–252.
[37] K. Engelborghs, T. Luzyanina, and G. Samaey, in *Technical Report TW-330* (Department of Computer Science, K. U. Leuven, Leuven, Belgium, 2001).
[38] MATLAB, http://www.mathworks.com (2005).
[39] D. J. Higham, SIAM Rev. **43**, 525 (2001).
[40] X. Huang, W. C. Troy, Q. Yang, H. Ma, C. R. Laing, S. J. Schiff, and J.-Y. Wu, J. Neurosci. **24**, 9897 (2004).
[41] M. L. V. Quyen, V. Navarro, J. Martinerie, M. Baulac, and F. J. Varela, Epilepsia **44**, 30 (2003).
[42] K. K. Jerger, S. L. Weinstein, T. Sauer, and S. J. Schiff, Clin. Neurophysiol. **116**, 545 (2005).
[43] D. T. J. Liley, private communication (2005).
[44] T. M. Clay and T. C. Ferree, IEEE Trans. Biomed. Eng. **21**, 629 (2002).
[45] B. Gordon, R. P. Lesser, N. E. Rance, J. Hart Jr., R. Webber, S. Uematsu, and R. S. Fisher, Electroencephalogr. Clin. Neurophysiol. **75**, 371 (1990).
[46] S. S. Nathan, S. R. Sinha, B. Gordon, R. P. Lesser, and N. V. Thakor, Electroencephalogr. Clin. Neurophysiol. **86**, 183 (1993).
[47] S. Wiggins, *Introduction to applied nonlinear dynamical systems and chaos* (Springer, New York, 2003).